Research Article

optica

Tight real-time synchronization of a microwave clock to an optical clock across a turbulent air path

HUGO BERGERON,[1,2*] LAURA C. SINCLAIR,[1] WILLIAM C. SWANN,[1] CRAIG W. NELSON,[1] JEAN-DANIEL DESCHÊNES,[1,2] ESTHER BAUMANN,[1] FABRIZIO R. GIORGETTA,[1] IAN CODDINGTON,[1] AND NATHAN R. NEWBURY[1*]

[1]National Institute of Standards and Technology, 325 Broadway, Boulder, CO, 80305, USA
[2]Université Laval, 2325 Rue de l'Université, Québec, QC, G1V 0A6, Canada
*Corresponding authors: hugo.bergeron@nist.gov, nathan.newbury@nist.gov

Received XX Month XXXX; revised XX Month, XXXX; accepted XX Month XXXX; posted XX Month XXXX (Doc. ID XXXXX); published XX Month XXXX

The ability to distribute the precise time and frequency from an optical clock to remote platforms could enable future precise navigation and sensing systems. Here we demonstrate tight, real-time synchronization of a remote microwave clock to a master optical clock over a turbulent 4-km open air path via optical two-way time-frequency transfer. Once synchronized, the 10-GHz frequency signals generated at each site agree to 10^{-14} at one second and below 10^{-17} at 1000 seconds. In addition, the two clock times are synchronized to ±13 fs over an 8-hour period. The ability to phase-synchronize 10-GHz signals across platforms supports future distributed coherent sensing, while the ability to time-synchronize multiple microwave-based clocks to a high-performance master optical clock supports future precision navigation/timing systems.

OCIS codes: *(120.3940) Metrology; (060.4510) Optical Communications*

http://dx.doi.org/10.1364/optica.x

1. Introduction

The distribution of time and frequency across a network enables applications such as navigation, coherent multi-static radar, communications and very-long-baseline interferometry. In the past, these applications have relied on microwave-based time-frequency transfer between microwave-based clocks. However, optically-based time-frequency transfer over fiber and free-space has the potential for over a thousand times higher performance [1–10]. Recently, we demonstrated optically-based two-way time-frequency transfer (O-TWTFT) for comparison between the times of two distant optical clocks over turbulent free-space paths [7]. Moreover, because of the very high bandwidth and precision of O-TWTFT, it was possible to tightly synchronize the two optical clocks to identical times to better than a femtosecond over hours and better than 20 femtoseconds over days [11].

Here we demonstrate synchronization between an optical clock and a remote microwave clock. We use the O-TWTFT approach of Ref. [11], but significantly modified, to support optical-to-microwave synchronization. The motivation to synchronize a microwave rather than an optical clock is twofold. First, while state-of-the-art microwave oscillators (e.g. quartz and dielectric resonator oscillators) have lower precision than optical oscillators (e.g. cavity-stabilized lasers), they are less expensive, smaller, more robust, and have lower power requirements by orders of magnitude. Second, many time-sensitive applications make use of a microwave signal, for example in the X-band at 10 GHz, which was not available in the all-optical system of Ref. [11]. A microwave clock at the remote sites can supply this required signal directly, efficiently, and at high signal power. In future time networks, optical-to-microwave synchronization would enable fieldable master optical atomic clocks [12] to distribute time across a network of much simpler microwave-based clocks while maintaining the absolute accuracy of the master. As conceptually illustrated in Fig. 1a, applications to other distributed coherent systems include multi-static synthetic aperture radar [13], precise time-resolved synchrotron measurements [14], very-long-baseline interferometry and radio-astronomy [15–18], pulse-position-modulation communication [19], or distribution of time to mobile platforms in a GPS-denied situation. In general, tight synchronization of a microwave clock is made difficult by its much greater timing noise than an optical clock. In GPS-disciplined oscillators, this timing noise is suppressed to the nanosecond level; here, we suppress this noise to the femtosecond level.

As shown in Fig. 1b, we synchronize our microwave clock to the optical clock over a folded 4 km long turbulent air path. Each clock outputs both a time signal via labelled optical pulses from a local frequency comb and a separate rf frequency signal at 10 GHz. Here, we use the term "clock" to refer to the generation of a local timebase rather than an absolute international timescale. It refers to the combination of frequency comb, oscillator, and controller (Fig 1b) that produces a

phase-coherent output of labelled pulses, i.e. "ticks", to define this local timebase; we are concerned with the difference between two such relative timescales. With modifications of the system, the master site could also be disciplined to an absolute timescale.

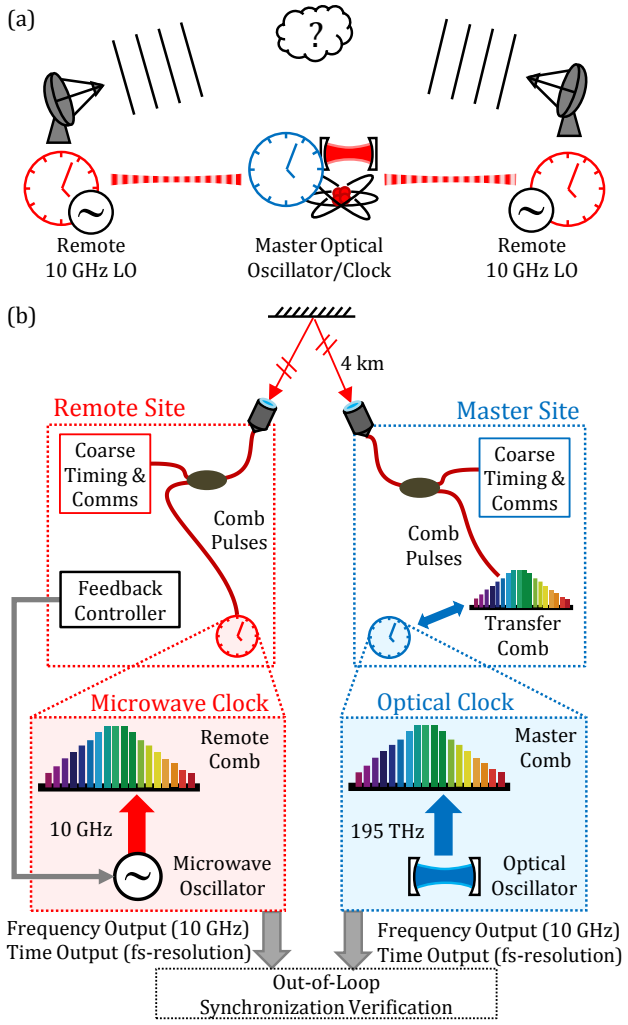

Fig 1. (a) Conceptual multi-static synthetic aperture radar where an array of microwave oscillators are synchronized to a single master optical oscillator. LO: local oscillator (b) The master site's clock is based on a laser stabilized to an optical cavity (optical oscillator). The remote site's clock is based on a combined quartz oscillator and dielectric resonator oscillator (DRO). This remote microwave clock is tightly synchronized to the optical clock over a folded 4 km long air path via O-TWTFT. The time and the frequency outputs from each clock are compared in a separate measurement to verify femtosecond time offsets and high phase coherence of the synchronized signals.

An "out-of-loop" comparison of the time signals shows a time deviation (tdev) below 10 femtoseconds for integration times ranging from 0.01 seconds to 1000 seconds, reaching values as low as 200 attoseconds. This time deviation increases in the presence of turbulence-induced dropouts because of the random walk of the microwave clock. However, it remains below 10 fs at ~85% link availability. A comparison of the 10-GHz frequency signals shows a similarly high level of coherence; the frequency difference, as measured by the modified Allan deviation, is 10^{-14} at 1 s and drops to below 10^{-17} at 1000 s. Within the 100-Hz synchronization bandwidth, the differential phase noise between the 10-GHz signals is reduced resulting in a 110-dB suppression at a 1-mHz Fourier frequency. The integrated differential phase noise is 375 μrad from 100 Hz to 100 μHz. This integrated phase noise corresponds to 6 fs of timing jitter, which is 3×10^5 times lower than the 2-ns jitter of the free-running microwave clock integrated over the same bandwidth. This phase coherence at 10 GHz is maintained despite a free-space link that suffers from turbulence-induced dropouts. To summarize, the demonstrated optical-to-microwave clock synchronization performance is comparable to optical-to-optical clock synchronization, in the limit of no turbulence-induced dropouts. Moreover, it provides highly phase-coherent 10-GHz signals, which were not available in the all-optical system [11].

We note that the synchronization rests on the previously demonstrated ability of the frequency comb to coherently convert phase between the microwave and optical domains. This capability is already used in optical frequency division to create extremely stable microwave frequencies [20–23]. Here, the system exploits the frequency comb for optical-microwave coherence over a distributed system. Critically, the timing information is carried by high-bandwidth optical signals, which enables the high precision and rapid feedback required to phase-stabilize a remote microwave clock. The remote microwave clock does require a co-located optical frequency comb, but current frequency combs, such as those in Ref. [24], are more compact and robust than optical oscillators (cavity-stabilized lasers).

2. Experimental Setup

Figure 2 provides an overview of the system. At the master site, a compact, self-referenced fiber frequency comb [24] is phase-locked to a cavity-stabilized laser with a residual pulse timing jitter of a few femtoseconds. The frequency comb produces a near-infrared optical pulse train with 200-MHz repetition frequency whose pulses are "labeled" by a local field-programmable gate array (FPGA) controller with respect to their arrival at a calibrated reference plane to define a local time. In addition, the 50th harmonic of the comb repetition frequency is detected to generate a 10-GHz frequency signal. (The exact choice of microwave frequency will depend on the application.)

At the microwave-clock site, a self-referenced frequency comb is phase-locked to a 10-GHz microwave oscillator via the 50th harmonic of its repetition frequency. (Details on the microwave clock architecture are presented in the supplemental material.) This labelled 200-MHz optical pulse train then provides an optical time output, just as is done at the master site. This clock remains a microwave clock since its timing rests on the underlying compact and inexpensive microwave oscillator rather than a much larger cavity-stabilized laser.

To synchronize the clocks, their time offset must be measured. Although we synchronize a microwave clock, the measurement of the time offset to femtosecond precision is done optically through O-TWTFT [7,11]. O-TWTFT relies on the reciprocity of a single-transverse-mode spatial link to cancel out turbulence and platform-induced variations in the path length and extracts the underlying clock time offsets. There are three basic subsystems: a comb-based two-way time-frequency transfer, a "coarser" two-way time-frequency transfer via a pseudo-random binary sequence (PRBS) imposed on an optical cw carrier, and a two-way optical communication channel for exchange of timing information. The coarser two-way transfer is necessary to resolve the 5-ns ambiguity of the 200-MHz comb pulses and to provide a coarse path delay measurement. The comb-based time transfer uses a linear optical sampling approach [25] to detect the pulse arrival times with femtosecond-level resolution. This linear optical sampling requires a third "transfer" comb located at the master clock site with a repetition frequency offset by Δf_r relative to the master comb.

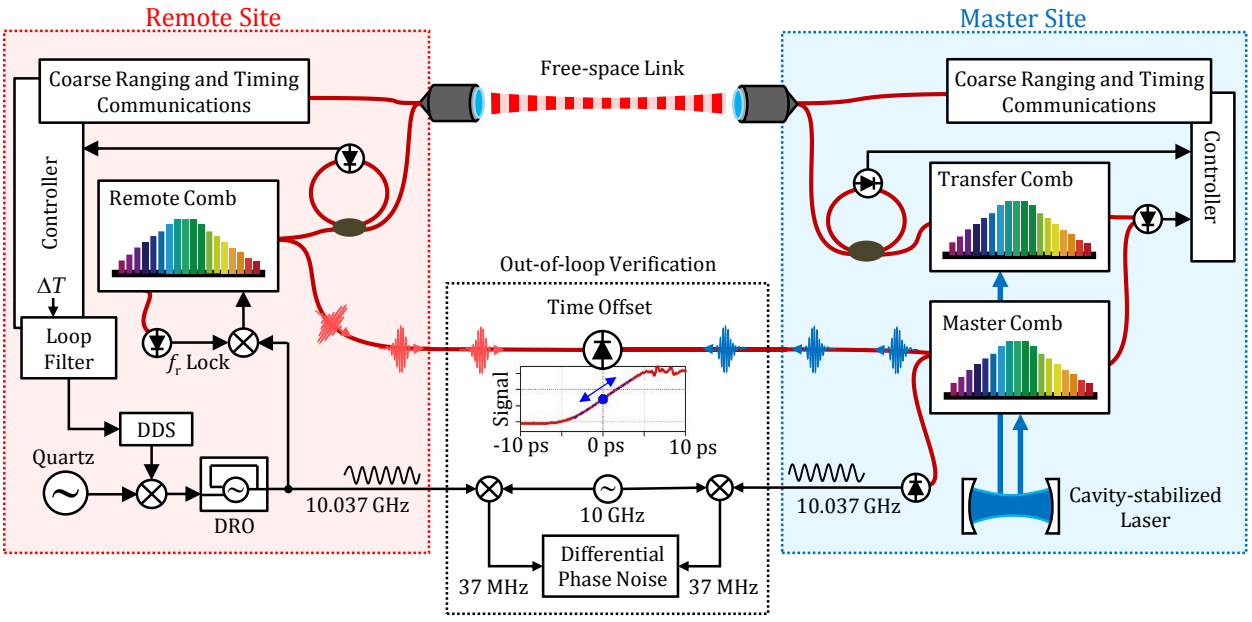

Figure 2: Schematic of the experimental setup. A master optical clock (blue shaded region) consists of a frequency comb phase-locked to a 195-THz cavity-stabilized laser. A remote synchronized microwave-based clock (red shaded region) consists of a frequency comb phase-locked to a 10-GHz oscillator. Each site produces a 10.037-GHz frequency output. At the master optical clock site, this 10-GHz signal corresponds to the 50th harmonic of the 200-MHz repetition rate frequency comb and is generated by optical frequency division. At the microwave clock site, it is the direct output of a quartz/DRO microwave oscillator. At both sites, the time output is defined by the arrival of the labelled optical pulses from the respective frequency combs at a common reference plane. (This step requires a separate calibration with a shorted link.) The two clocks are synchronized by a Kalman-filter-based loop filter that uses the input time offset, as measured through O-TWTFT, to steer the frequency of the DRO. DDS: direct digital synthesizer; f_r: repetition frequency of the frequency comb.

Here, we have modified the O-TWTFT system of Ref. [11] in three significant ways to allow optical-to-microwave clock synchronization. First, the microwave clock is constructed to maintain tight phase coherence between the microwave oscillator and local frequency comb used in the time transfer. (See Supplemental section.) The timing corrections returned from the O-TWTFT are applied directly to the 10-GHz oscillator so that its output follows the master site at low Fourier frequencies but retains the low phase noise of the dielectric resonator oscillator (DRO) at high Fourier frequencies, which is useful in applications such as synthetic aperture radar and phased-array systems where timing jitter at high offset frequencies degrades performance. Second, the effective overall feedback bandwidth has been increased tenfold to suppress the much higher random walk of the microwave oscillator compared to an optical oscillator. Third, the feedback is applied by a Kalman-filter-based loop filter for optimal hold-over performance during a turbulence-induced dropout.

For the comb-based two-way transfer, the combs are operated at a repetition frequency of $f_r \approx 200$ MHz with the transfer comb's repetition rate offset by $\Delta f_r \approx 2$ kHz. The comb pulses are filtered to a 1.5 THz spectral bandwidth centered at 1560 nm. An average power of 5 mW (2×10^8 photons per pulse) is launched across the 4-km folded open air path from both sites. The folded 4-km path is achieved through use of two 53-cm diameter flat mirrors separated by 1 km. Optical pathlength variations from mirror motion, just as those from turbulence, are removed by the two-way measurement. 2.5-cm aperture custom low-insertion-loss free-space optical terminals with tip/tilt correction are used to maximize the link availability, i.e. the amount of time the received power is above the detection threshold. The received power varied between 0 nW and 3.8 μW and was below 370 nW for 99% of the time. The detection threshold, the minimum received power for which the in-loop time offset can be computed, was set to 2.5 nW, corresponding to 96 photons per comb pulse. To operate over even longer air paths with similar link availability, a higher launch power will be required to overcome the increased diffraction and integrated turbulence. Also, the increased time-of-flight associated with longer air paths will degrade the two-way reciprocity but it has been shown this effect will have negligible impact on the two-way time-frequency transfer [26].

The coarser two-way time-frequency transfer and communication link are both implemented by phase modulation of a 5-mW 1536-nm cw laser. This light is then wavelength multiplexed with the comb and co-propagated to the other site where it is heterodyned against the local cw laser and demodulated. For coarse two-way time-frequency transfer, a PRBS modulation is used, while for communication, binary phase-shift keying (BPSK) is used, both operating at 10 Mbps. Communication packets are interposed between adjacent coarse two-way time measurements within a single time interval of length $1/\Delta f_r$.

The communication link transfers the timing data from the master optical-clock site to the remote microwave-clock site. An FPGA-based controller at the microwave-clock site then computes the time offset between the two clocks, ΔT, from the O-TWTFT master synchronization equation (Equation (1) of Ref. [11]) every $1/\Delta f_r \approx 0.5$ ms, as long as there is no turbulence-induced dropout. This time offset is input to a Kalman-filter-based loop filter whose output controls the microwave-oscillator frequency via a direct digital synthesizer (DDS). (See the next section and the supplemental section for more details.) The overall synchronization bandwidth was set at 100 Hz by empirically minimizing the residual timing jitter.

As the overall system is essentially a spatially distributed phase-locked loop, it necessarily drives the measured in-loop time offset, ΔT, to zero. It is therefore critical to verify synchronization through separate out-of-loop measurements, which is possible here through the use of a folded air path (See Fig. 1b). Moreover, the synchronized time outputs and frequency outputs must be separately measured. As shown in Fig. 2, the 10.037-GHz frequency outputs are down-mixed by a common 10-GHz stable oscillator to match the input bandwidth of the phase measurement test system [27].

The time offsets of the 200-MHz pulse trains are measured through the amplitude variation of their demodulated optical interference [11]. A 1-MHz heterodyne signal from the two pulse trains is obtained by shifting the carrier-envelope-offset frequency of the remote comb. This demodulated signal is shown as the "Time Offset" inset in Fig. 2, where the blue dot indicates "zero" calibrated time offset. Any deviations in amplitude from this zero point reflect time offsets between the clocks. This approach allows for time offset measurements within a range of ±5 ps, based on the choice of optical filters, and femtosecond uncertainty. Direct photodetection of each signal is also possible but will introduce additional time uncertainty. These signals would form the time output of the clock to be used in a real-world application. It is also possible to pulse pick these time signals for a lower rate time signal than 200 MHz, depending on the application.

3. Synchronization Across Turbulence-induced Dropouts

Atmospheric turbulence causes distortions of the beam across the link and thus fluctuations in the received power. Because O-TWTFT requires a single spatial-mode optical link to ensure reciprocity [28], the fluctuations are relatively strong compared with a multi-mode link. Depending on transmitted power, turbulence strength, and distance, these turbulence-induced fluctuations can sometimes cause the received power to fall below the detection threshold, causing a dropout. The statistics of the dropout frequency and duration will depend on the exact conditions (i.e. turbulence strength, launched power, detection threshold, aperture diameter) and have been analyzed extensively in the context of free-space laser communications [29]. When a dropout occurs, the measured time offset is not updated. Microwave-to-optical synchronization puts greater demands on the system than optical-to-optical synchronization due to the larger excursions of microwave oscillators during these dropouts. The naïve approach of a sample-and-hold leads to runaway behavior. A Kalman-filter-based approach provides close to optimal hold-over behavior [30].

Figure 3a shows the implemented loop filter based on a Kalman filter whose state vector contains two variables. The filter performs an estimation of the phase and frequency error between the clocks using intermittent time offset measurements provided by the O-TWTFT system. When a measurement is available, the internal estimate of the timing error is updated using feedback gain factors that depend on the dropout length and an a priori noise model. White (f^0) measurement noise and frequency random walk (f^{-4}) oscillator phase-noise are assumed here. To ease the implementation of the loop filter on the FPGA, the feedback gain as a function of measurement interval was pre-computed and stored in a look-up table.

Figures 3b and 3c show the performance across relatively long dropouts of 50 ms. (Dropouts due to atmospheric turbulence usually last less than 10 ms under our operating conditions [11]). For most dropouts, the timing error due to the random walk of the microwave clock is below the high-frequency timing-jitter, yet for longer dropouts there can sometimes be a significant excess deviation. The rapid recoveries from the excess deviations will appear in the phase-noise power spectral density (PSD) as an increased white noise floor below the synchronization feedback bandwidth (see Fig. 6). Since the remote controller has knowledge of the dropouts, a distributed system could operate in either "gated operation", only during periods of fully established synchronization, or in continuous mode that includes periods of dropouts. Here, in gated operation, data is masked during the period of a dropout until the in-loop time offset becomes available again and falls below a threshold. (The threshold is chosen to be 2σ of the instantaneous in-loop time offset.)

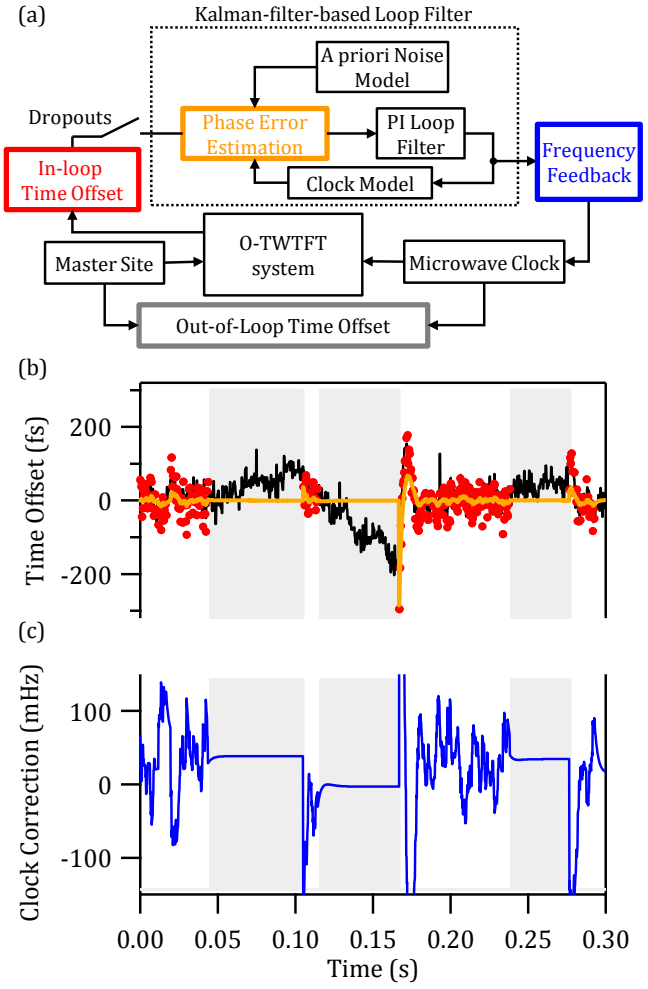

Fig. 3. System operation during dropouts. (a) Schematic of the Kalman-filter-based loop filter. PI: proportional and integral (b) The measured out-of-loop time offset (black trace), in-loop time offset measured via the O-TWTFT system (red circles), and predicted in-loop timing offset from the loop filter (orange trace). During the shaded gray regions, the received power over the single-mode link was below threshold, leading to a dropout in the measured in-loop time offset. (c) The correction applied to the frequency of the 10-GHz signal (blue trace).

4. Performance

To test the synchronization, the system was operated continuously over an 8-hour period across the 4-km folded link. During this period, the synchronization was verified for both the time and frequency outputs of the clocks. In addition, the link availability, clock correction signals, and turbulence strength were also monitored. The measurement was stopped when shifts in the mirrors used to fold the optical path caused a very long dropout. (The free-space terminals include tip/tilt corrections to correct for temperature and turbulence-induced variations in pointing, but the folding mirrors have no active correction.) Figure 4 shows a partial data set including the out-of-loop time offset, link availability, and turbulence strength averaged over a 1-second window. The average link availability was 85% but varied significantly over the run depending on turbulence strength and the alignment of the folding mirrors. The time offset is discussed in more detail below.

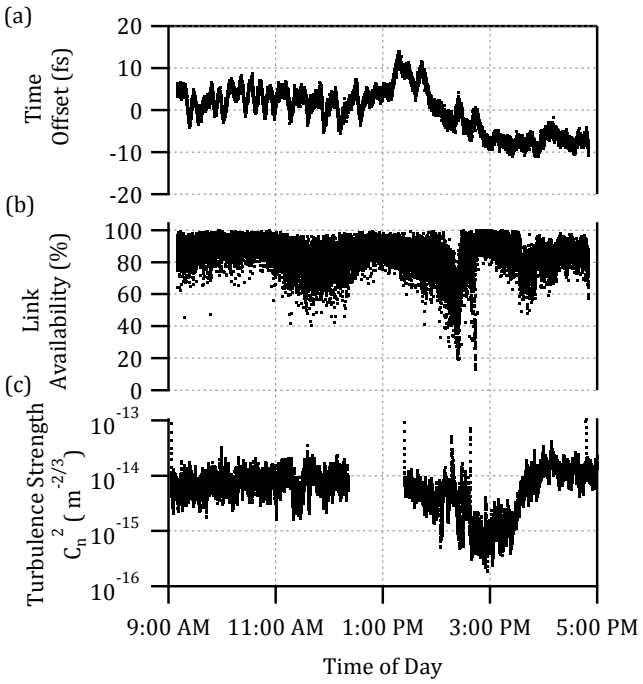

Fig. 4. (a) Time offset (gated operation) between the optical and microwave clocks. (b) Link availability. (c) Turbulence strength as measured by the turbulence structure function C_n^2. All data is averaged over a one second window.

A. Time outputs: Femtosecond time synchronization

The time between the two clocks is verified via the arrival of their optical pulses at a common reference plane (Fig. 2). Figure 4a shows the time offset for gated operation. Figure 5 shows the time deviation derived from these data for gated operation and also for continuous operation. The time deviation for continuous operation is below 10 fs for time periods ranging from 1000 s down to 0.01 s. The time deviation for gated operation is also below 10 fs reaching a minimum of 200 attoseconds at a 10 second averaging time. Finally, the overall variation in the time offset across 8 hours, shown in Fig. 4, is below ±13 fs. This variation is dominated by laboratory temperature variations that cause path length changes in the ~1 m fiber-optic paths used in the out-of-loop measurements as well as elsewhere in the transceivers. This temperature dependence can be seen in the slow 20-minute oscillations of Fig. 4a, which match the cycling of the room air conditioning.

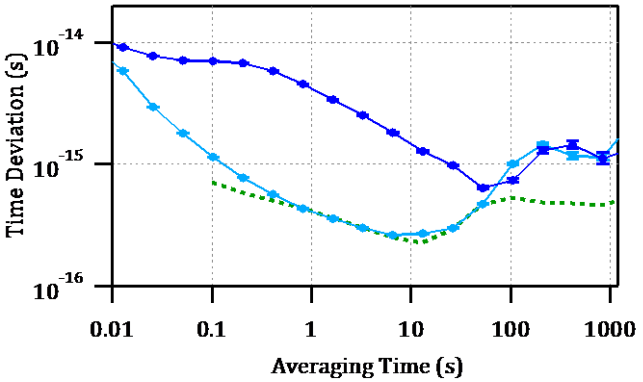

Fig. 5. Time deviation calculated from the measured time offset between the microwave and optical clock for gated operation (light blue curve) and for continuous operation (dark blue curve). The data for gated operation agrees with previous optical-to-optical synchronization (dashed green curve) [11] out to 100 s.

Both the time offset of Fig. 4a and the time deviation for gated operation of Fig. 5 are in good quantitative agreement with the previous optical-to-optical synchronization [11]. Therefore, there is no degradation in the time synchronization associated with the conversion of the remote clock from optical to a microwave oscillator beyond the unavoidable excess time wander that occurs during dropouts.

B. Frequency outputs: Synchronized 10 GHz signals

The 10-GHz microwave frequency signals are also compared during the 8-hour run by measuring their phase difference, as shown in Fig. 2. In this case, the phase measurement test system [27] only allows for continuous comparison of 10-GHz signals rather than gated operation. These phase-difference data yield a phase-noise PSD that quantifies the relative phase coherence or an Allan deviation that quantifies the relative frequency difference. We discuss both here. In addition, we can compare the coherence of the microwave signal to that of the optical pulse train.

Figure 6 shows the single-side-band PSD between the two sites for the case of a free-running microwave clock (purple line) and synchronized microwave clock across the turbulent 4 km link (red line). At low offset frequencies, the suppression of the free-running oscillator noise is significant, reaching 110 dB at a 1-mHz offset frequency. (Below a 1-Hz offset frequency, the synchronized 10-GHz phase-noise is also below that of a free-running optical cavity.) This dramatic suppression of phase noise at low offset frequencies leads to a corresponding reduction in the integrated timing jitter. The timing jitter for the synchronized system is 6 fs integrated from the 100 Hz synchronization bandwidth to 100 μHz, compared to greater than 2 ns for the free running case.

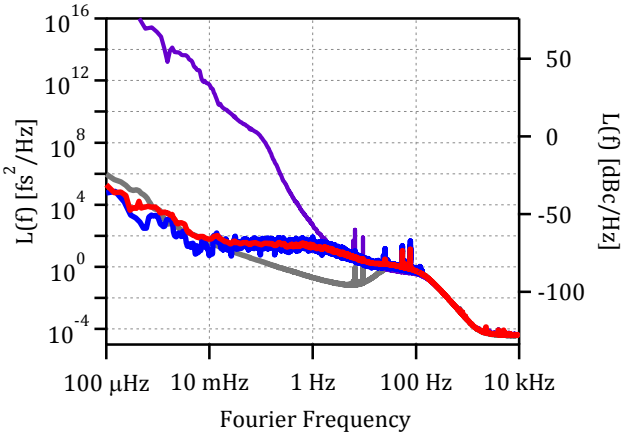

Fig. 6. Single-side-band power spectral density (PSD) for differential phase noise of the 10 GHz outputs from the optical and microwave clocks without synchronization (purple curve), while synchronized over the 4 km link (red curve), and while synchronized over a shorted link (grey curve). The integrated phase noise is 375 μrad (6 fs) for the red curve from 100 μHz out to the synchronization bandwidth of 100 Hz. In addition, the PSD calculated from the optical time outputs is shown (in blue).

Figure 6 also shows the differential phase noise for a synchronized system over a shorted link (grey line), rather than over 4 km. There is an increase in phase noise for the 4-km synchronization at offset frequencies from 10 Hz to 10 mHz, which is attributed to dropouts and not to a lack of reciprocity across the link. As discussed in Section 3, dropouts occur only briefly and appear as wideband noise on the PSD, extending up to the synchronization bandwidth.

Finally, Figure 6 shows the scaled phase noise from the optically measured time offset signals (blue line). The direct 10-GHz measurement exhibits a slightly higher phase noise than the optical measurement at low Fourier frequencies due to f^{-1} noise associated with the microwave test setup. (See Supplemental section.)

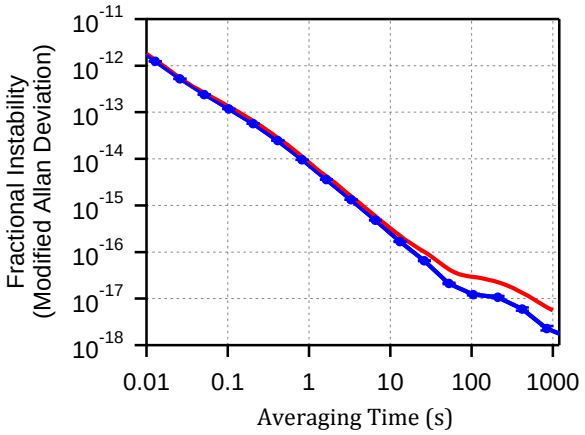

Fig. 7. Fractional instability (modified Allan deviation) of the frequency difference between the remote sitea nd master site clocks during continuous operation for the synchronized 10-GHz microwave outputs (red trace) and for the optical time offsets (blue trace).

Figure 7 presents the relative fractional frequency difference between the microwave and optical clocks in terms of the modified Allan deviation. The 10-GHz microwave signals agree to below 1×10^{-14} at a 1-s averaging time and below 1×10^{-17} at a 1000-s averaging time. Note that the master 10-GHz signal is not tied to an atomic reference but rather drifts slowly with the underlying optical cavity. However, for many sensing applications, the important parameter is the relative frequency stability of the microwave signal between clock nodes rather than the absolute frequency. If better long term frequency stability is required, an atomic clock could be used at the master site. At long averaging times there is a slight degradation compared to the values based on the optical time output (blue line). This degradation again reflects the additional excess f^{-1} noise as in the PSD of Fig. 6.

5. Conclusions

We report the synchronization of a microwave oscillator to an optical oscillator over a 4-km turbulent free-space link. The residual time deviation is below 10 fs with a long-time variation that remains below ±13 fs over 8 hours. We find similar phase coherence between the synchronized 10-GHz frequency outputs with a residual frequency difference of 10^{-17} at 1000-s averaging. For greater phase-coherence at Fourier frequencies beyond the effective synchronization bandwidth of 100 Hz, the quartz-DRO pair could be replaced by an optical-frequency-division-generated signal [20–23] or a cryogenic sapphire oscillator [31,32]. The high coherence and full time synchronization demonstrated here could enable applications from time distribution to long-baseline radio astronomy. If extended to moving platforms by appropriate compensation for Doppler shifts, this technique could similarly enable applications such as precise formation flying of phased satellite-arrays.

Funding. We acknowledge funding from the DARPA DSO PULSE program and from NIST.

Acknowledgment. We thank Dave Howe and Kevin Cossel for helpful comments and Archita Hati and Michael Cermak for technical assistance.

See Supplement 1 for supporting content.

REFERENCES

1. G. Lutes and A. Kirk, *Reference Frequency Transmission Over Optical Fiber*, The Telecommunications and Data Acquisition Report (Jet Propulsion Laboratory, 1986).
2. L.-S. Ma, P. Jungner, J. Ye, and J. L. Hall, "Delivering the same optical frequency at two places: accurate cancellation of phase noise introduced by an optical fiber or other time-varying path," Opt. Lett. **19**, 1777–1779 (1994).
3. N. R. Newbury, P. A. Williams, and W. C. Swann, "Coherent transfer of an optical carrier over 251 km," Opt Lett **32**, 3056–3058 (2007).
4. E. Samain, P. Exertier, P. Guillemot, F. Pierron, D. Albanese, J. Paris, J.-M. Torre, I. Petitbon, and S. Leon, "Time transfer by laser link T2L2 first results," in *Frequency Control Symposium, 2009 Joint with the 22nd European Frequency and Time Forum. IEEE International* (2009), pp. 194 –198.
5. K. Djerroud, O. Acef, A. Clairon, P. Lemonde, C. N. Man, E. Samain, and P. Wolf, "Coherent optical link through the turbulent atmosphere," Opt. Lett. **35**, 1479–1481 (2010).
6. L. Sliwczynski, P. Krehlik, L. Buczek, and M. Lipinski, "Frequency Transfer in Electronically Stabilized Fiber Optic Link Exploiting Bidirectional Optical Amplifiers," IEEE Trans. Instrum. Meas. **61**, 2573–2580 (2012).
7. F. R. Giorgetta, W. C. Swann, L. C. Sinclair, E. Baumann, I. Coddington, and N. R. Newbury, "Optical two-way time and frequency transfer over free space," Nat. Photonics **7**, 434–438 (2013).
8. S. Droste, F. Ozimek, T. Udem, K. Predehl, T. W. Hänsch, H. Schnatz, G. Grosche, and R. Holzwarth, "Optical-Frequency Transfer over a Single-Span 1840 km Fiber Link," Phys. Rev. Lett. **111**, 110801 (2013).
9. O. Lopez, F. Kéfélian, H. Jiang, A. Haboucha, A. Bercy, F. Stefani, B. Chanteau, A. Kanj, D. Rovera, J. Achkar, C. Chardonnet, P.-E. Pottie, A. Amy-Klein, and G. Santarelli, "Frequency and time transfer for metrology and beyond using telecommunication network fibres," Comptes Rendus Phys. **16**, 531–539 (2015).
10. S. Droste, C. Grebing, J. Leute, S. M. F. Raupach, A. Matveev, T. W. Hänsch, A. Bauch, R. Holzwarth, and G. Grosche, "Characterization of a 450 km baseline GPS carrier-phase link using an optical fiber link," New J. Phys. **17**, 083044 (2015).
11. J.-D. Deschenes, L. C. Sinclair, F. R. Giorgetta, W. C. Swann, E. Baumann, H. Bergeron, M. Cermak, I. Coddington, and N. R. Newbury, "Synchronization of Distant Optical Clocks at the Femtosecond Level," PRX (2016, in press).
12. K. Bongs, Y. Singh, L. Smith, W. He, O. Kock, D. Swierad, J. Hughes, S. Schiller, S. Alighanbari, S. Origlia, S. Vogt, U. Sterr, C. Lisdat, R. L. Targat, J. Lodewyck, D. Holleville, B. Venon, S. Bize, G. P. Barwood, P. Gill, I. R. Hill, Y. B. Ovchinnikov, N. Poli, G. M. Tino, J. Stuhler, W. Kaenders, and the S. team, "Development of a strontium optical lattice clock for the SOC mission on the ISS," Comptes Rendus Phys. **16**, 553–564 (2015).
13. Z. Li, L. Yan, Y. Peng, W. Pan, B. Luo, and L. Shao, "Phase fluctuation cancellation of anonymous microwave signal transmission in passive systems," Opt. Express **22**, 19686 (2014).
14. R. Wilcox, J. M. Byrd, L. Doolittle, G. Huang, and J. W. Staples, "Stable transmission of radio frequency signals on fiber links using interferometric delay sensing," Opt. Lett. **34**, 3050 (2009).
15. M. Calhoun, R. Sydnor, and W. Diener, "A stabilized 100-megahertz and 1-gigahertz reference frequency distribution for Cassini Radio Science," Interplanet. Netw. Prog. Rep **148**, 1–11 (2001).
16. J.-F. Cliche and B. Shillue, "Precision timing control for radioastronomy: maintaining femtosecond

synchronization in the Atacama Large Millimeter Array," IEEE Control Syst. **26**, 19–26 (2006).
17. S. S. Doeleman, J. Weintroub, A. E. E. Rogers, R. Plambeck, R. Freund, R. P. J. Tilanus, P. Friberg, L. M. Ziurys, J. M. Moran, B. Corey, K. H. Young, D. L. Smythe, M. Titus, D. P. Marrone, R. J. Cappallo, D. C.-J. Bock, G. C. Bower, R. Chamberlin, G. R. Davis, T. P. Krichbaum, J. Lamb, H. Maness, A. E. Niell, A. Roy, P. Strittmatter, D. Werthimer, A. R. Whitney, and D. Woody, "Event-horizon-scale structure in the supermassive black hole candidate at the Galactic Centre," Nature **455**, 78–80 (2008).
18. S. Doeleman, T. Mai, A. E. E. Rogers, J. G. Hartnett, M. E. Tobar, and N. Nand, "Adapting a Cryogenic Sapphire Oscillator for Very Long Baseline Interferometry," Publ. Astron. Soc. Pac. **123**, 582–595 (2011).
19. J. Sushchik M., N. Rulkov, L. Larson, L. Tsimring, H. Abarbanel, K. Yao, and A. Volkovskii, "Chaotic pulse position modulation: a robust method of communicating with chaos," IEEE Commun. Lett. **4**, 128–130 (2000).
20. T. M. Fortier, M. S. Kirchner, F. Quinlan, J. Taylor, J. C. Bergquist, T. Rosenband, N. Lemke, A. Ludlow, Y. Jiang, C. W. Oates, and S. A. Diddams, "Generation of ultrastable microwaves via optical frequency division," Nat. Photon **5**, 425–429 (2011).
21. A. Haboucha, W. Zhang, T. Li, M. Lours, A. N. Luiten, Y. Le Coq, and G. Santarelli, "Optical-fiber pulse rate multiplier for ultralow phase-noise signal generation," Opt. Lett. **36**, 3654 (2011).
22. A. Hati, C. W. Nelson, C. Barnes, D. Lirette, T. Fortier, F. Quinlan, J. A. Desalvo, A. Ludlow, S. A. Diddams, and D. A. Howe, "State-of-the-art RF signal generation from optical frequency division," IEEE Trans. Ultrason. Ferroelectr. Freq. Control **60**, 1796–1803 (2013).
23. F. Quinlan, F. N. Baynes, T. M. Fortier, Q. Zhou, A. Cross, J. C. Campbell, and S. A. Diddams, "Optical amplification and pulse interleaving for low-noise photonic microwave generation," Opt. Lett. **39**, 1581 (2014).
24. L. C. Sinclair, J.-D. Deschênes, L. Sonderhouse, W. C. Swann, I. H. Khader, E. Baumann, N. R. Newbury, and I. Coddington, "Invited Article: A compact optically coherent fiber frequency comb," Rev. Sci. Instrum. **86**, 081301 (2015).
25. I. Coddington, W. C. Swann, and N. R. Newbury, "Coherent linear optical sampling at 15 bits of resolution," Opt. Lett. **34**, 2153–2155 (2009).
26. C. Robert, J.-M. Conan, and P. Wolf, "Impact of turbulent phase noise on frequency transfer with asymmetric two-way ground-satellite coherent optical links," PRA (2016, in press).
27. Symmetricom Model 5125A. The use of trade names is necessary to specify the experimental results and cannot imply endorsement by the National Institute of Standards and Technology.
28. J. H. Shapiro, "Reciprocity of the Turbulent Atmosphere," J Opt Soc Am **61**, 492–495 (1971).
29. L. C. Andrews, R. L. Phillips, and C. Y. Hopen, *Laser Beam Scintillation with Applications* (SPIE Press, 2001).
30. R. E. Kalman, "A New Approach to Linear Filtering and Prediction Problems," Trans. ASME–Journal Basic Eng. **82**, 35–45 (1960).
31. S. Grop, P.-Y. Bourgeois, R. Boudot, Y. Kersale, E. Rubiola, and V. Giordano, "10 GHz cryocooled sapphire oscillator with extremely low phase noise," Electron. Lett. **46**, 420–422 (2010).
32. N. R. Nand, J. G. Hartnett, E. N. Ivanov, and G. Santarelli, "Ultra-Stable Very-Low Phase-Noise Signal Source for Very Long Baseline Interferometry Using a Cryocooled Sapphire Oscillator," IEEE Trans. Microw. Theory Tech. **59**, 2978–2986 (2011).

Supplementary Material

optica

Tight real-time synchronization of a microwave clock to an optical clock across a turbulent air path: Supplementary Material

HUGO BERGERON,[1,2*] LAURA C. SINCLAIR,[1] WILLIAM C. SWANN,[1] CRAIG W. NELSON,[1] JEAN-DANIEL DESCHÊNES,[1,2] ESTHER BAUMANN,[1] FABRIZIO R. GIORGETTA,[1] IAN CODDINGTON,[1] AND NATHAN R. NEWBURY[1*]

[1]*National Institute of Standards and Technology, 325 Broadway, Boulder, CO, 80305, USA*
[2]*Université Laval, 2325 Rue de l'Université, Québec, QC, G1V 0A6, Canada*
**Corresponding authors: hugo.bergeron@nist.gov, nathan.newbury@nist.gov*

Published XX Month XXXX

This document provides supplementary information to "Tight real-time synchronization of a microwave clock to an optical clock across a turbulent air path," *Optica* volume, first page (year). Here, we discuss details of the microwave clock and present a more detailed schematic.

http://dx.doi.org/10.1364/optica.99.099999.s1 [supplementary document doi]

It is important to maintain tight phase coherence between the microwave oscillator and the local frequency comb that comprises the microwave clock. The setup is illustrated schematically in Fig. S1. The microwave oscillator is a combination of a quartz oscillator and a dielectric resonator oscillator (DRO). A quiet 100-MHz quartz oscillator is frequency multiplied by a factor of 100. The DRO is phase-locked to this 10-GHz signal with about 100-kHz bandwidth to reduce the phase noise level at high Fourier frequencies and for greater frequency flexibility. A self-referenced frequency comb is then phase-locked to this signal by mixing the 10.037-GHz output of the Quartz/DRO pair with the detected 50th harmonic of the comb's repetition frequency in a low-noise mixer to create a baseband phase error signal. The digital loop filter (implemented on a field-programmable gate array (FPGA)) that controls these actuators uses a 16-bit ADC to measure the phase error signal and its gains are adjusted to reach a 10-kHz lock bandwidth. Piezoelectric actuators close the feedback loop by changing the repetition frequency of the comb by adjusting the cavity length of the comb. With the feedback loop closed, there are three coherent outputs, one optical and two rf: the optical 200-MHz pulse train, the 10.037-GHz signal generated from direct photodetection of the frequency comb pulses, and the 10.037-GHz signal from the DRO.

With the system described above, the frequency comb is tightly locked to the microwave oscillator. To achieve synchronization, the system then adjusts the phase of the microwave oscillator as described next. First, the time offset is computed from the O-TWTFT master synchronization equation [1] by an FPGA-based controller co-located with the microwave clock. This time offset acts as an in-loop error signal that is filtered (as discussed in Section 3) and then used to adjust the frequency of the microwave oscillator. The frequency adjustment is implemented through an offset lock of the DRO to the 10-GHz quartz signal, as shown in Fig. S1. The offset is provided by an adjustable low-noise direct digital synthesizer (DDS) module. A 37 MHz nominal DDS frequency was used, leading to a 10.037-GHz DRO output.

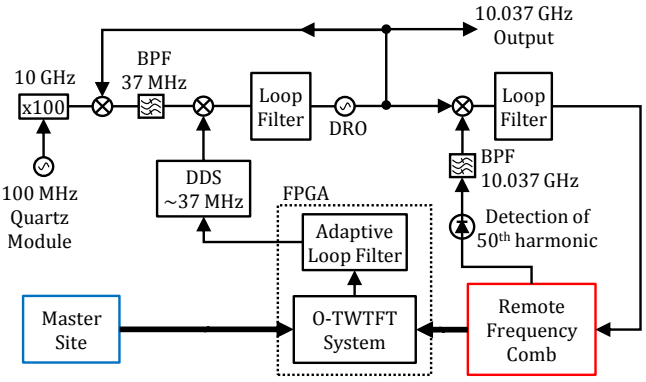

Fig. S1 Stabilization architecture for the microwave clock. BPF: bandpass filter, DRO: dielectric resonator oscillator, O-TWTFT: Optical two-way time-frequency transfer.

REFERENCES

1. J.-D. Deschenes, L. C. Sinclair, F. R. Giorgetta, W. C. Swann, E. Baumann, H. Bergeron, M. Cermak, I. Coddington, and N. R. Newbury, PRX (2016, in press).